Accurate Compact MOSFET Modeling Scheme for Harmonic Distortion Analysis

B. Iñiguez*, R. Picos**, I. Kwon***, M. S. Shur****, T. A. Fjeldly*****, and K. Lee***

Abstract—We discuss and develop a compact MOSFET modeling scheme in order to obtain accurate descriptions of the drain current and its derivatives up to the 5th order. We have analyzed the physical effects which govern the behaviour of the 3rd derivative in long and deep-submicron channel MOSFETs. Our modeling agrees well with experimental data and describes continuous transitions between operating regimes, thanks to the use of continuous functions, which do not introduce any artificial peaks.

I. INTRODUCTION

An adequate MOSFET model for distortion analysis should not only provide accurate current-voltage characteristics, but should also exhibit good agreement with higher order derivatives of the drain current, which determine the main contributions to higher-order harmonics [1-3]. Most MOSFET models do not satisfactorily describe distortion. One of the reasons is that the modeling equations of some physical effects, such as mobility, series resistance, and velocity saturation, are not sufficiently accurate for describing the derivatives. Another reason is that the interpolation

Manuscript received May 31, 2004; revised September 15, 2004.
    * DEEEA, Universitat Rovira i Virgili, Avda. Països Catalans 26, 43007 Tarragona Spain. E-mail: binyigue@etse.urv.es
    ** Department of Physics, Universitat de les Illes Balears, Cra. De Valldemossa, Km. 755, 07071 Palma de Mallorca, Spain
    *** Department of Electrical Engineering and Computer Science, KAIST, Taejon, 305-701Korea
    **** ECSE Department Rensselaer Polytechinc Institute, 110 8th Street, Troy, 12180NY, USA
    ***** UniK- University Graduate Center, 70 Postboks, Kjeller, N-2027, Norway

functions, used to provide smooth transitions between regimes, often induce artificial peaks and kinks when the modeled characteristics are differentiated.

A surface potential-based charge sheet model [4-7], can provide accurate expressions of harmonics up to the third order. However, in order to ease circuit design, it would be desirable to develop a model which could, at the same time, keep the physical basis of surface potential-based models and use simpler expressions which may allow direct parameter extraction techniques for most of the model parameters.

An alternative to surface potential-based models are the charge linearization models, which result from a linearization of the inversion charge density with respect to the surface potential [8-16]. This approach leads to simpler expressions of the drain current, total charges, and the small-signal parameters, and allows for easy incorporation of short-channel effects needed to model scaled-down devices, and for the development of direct techniques to extract most of the parameters [9]. Besides, the effect of the device parameters on the harmonic performance is easier to estimate.

In this paper, we present a compact model, based on charge linearization, which provides acceptable accuracy up to the 5th derivative of the drain current. This model follows the approach used by previous charge linearization models, such as UCCM [11-14] and EKV v2.6 [9], but its accuracy for the nth derivatives is increased thanks to the use of an appropriate mobility model (accounting for the main scattering mechanisms), a proper incorporation of short-channel effects (velocity saturation, channel-length modulation, DIBL, and series resistance), and the utilization of more adequate interpolation functions. The physical basis of the model

allows for easy determination of the influence of each physical effect on the higher-order derivatives of the channel current, in particular on the 3rd derivatives. It is shown that some effects, such as velocity saturation and channel length modulation, make the shape of the 3rd derivative of a deep-submicron MOSFET very different from that for a long-channel device. We also demonstrate the problems of other conventional modeling techniques to accurately fit the experimental 3rd derivatives. In particular, it is shown that artificial peaks are often found. In contrast, our model provides reasonably good agreement with experimental results through all operating regimes for MOS transistors with effective channel lengths down to 0.11 μm.

II. MODEL

Our compact charge linearization model is based on the unified charge control model (UCCM). This model is derived from a charge-sheet model by linearizing the channel charge density in terms of the surface potential:

$$a(n_c - n_0) + \eta V_{th} \ln\left(\frac{n_c}{n_0}\right) = V_{GS} - V_T - \alpha V_{CS} \quad (1)$$

where η is the subthreshold ideality factor, V_{th} is the thermal voltage, V_T is the threshold voltage, n_c is the local (inversion) carrier density, V_{CS} is the channel voltage (referred to the source), α is the body effect parameter,

$n_0 = \dfrac{\eta V_{th} C_{ox}}{2q}$ and $a = \dfrac{q}{C_{ox}}$, C_{ox} being the oxide

capacitance per unit area. This charge control model reduces to the one used in EKV v2.6 model if V_T and α have the values resulting from the linearization of the inversion charge density at the substrate [17].

Equation (1) has no analytical solution for the inversion charge density. However, several approximate explicit expressions for the inversion charge density in terms of the voltage bias have been proposed. One of the most commonly used expressions is:

$$n_c = 2n_0 \log\left[1 + 0.5\exp\left(\frac{V_{GS} - V_T - \alpha V_{CS}}{\eta V_{th}}\right)\right] \quad (2)$$

However, these expressions ignore the increase of the surface potential with the gate voltage in strong inversion, which may affect the accuracy of the high order derivatives of the channel current. On the other hand, the effect of non-pinned surface potential in strong inversion is inherent to UCCM. Equation (1) can be solved for n_c in terms of the Lambert's W function:

$$n_c = 2n_0 \text{LambertW}\left(\frac{1}{2}\exp\left(\frac{1}{2} + \frac{V_{GS} - V_T}{\eta V_{th}}\right)\right) \quad (3)$$

Our channel current model is derived using the Gradual Channel Approximation, which is valid in the non-saturated part of the channel. In channel potential formulation, it can be written as:

$$I_{ds} = \mu W q n_c \frac{dV_{CS}}{dx} \quad (4)$$

In surface potential formulation, the drain current can be written as:

$$I_{ds} = Wq\left[-\mu V_{th}\frac{dn_c}{dx} + n_c v\right] \quad (5)$$

where v is the drift velocity.

The first term in (5) is the contribution due to diffusion and the second term is the contribution due to drift.

The drift velocity depends on the lateral field (field in the direction of the channel). At low lateral fields, it is proportional to the field; at high lateral fields it saturates to a value (v_{sat}). An appropriate and simple velocity-field relationship is the one proposed by Sodini, which is quite accurate for nMOSFETs.

$$v = \begin{cases} \dfrac{\mu_n E_x}{1 + \dfrac{\mu_n E_x}{2v_{sat}}} & E_x \le \dfrac{2v_{sat}}{\mu_n} \\ v_{sat} & E_x \ge \dfrac{2v_{sat}}{\mu_n} \end{cases} \quad (6)$$

where μ_n is the carrier mobility that depends on the normal fields, and E_x is the absolute value of the lateral field. It can be written as $E_x = \dfrac{d\psi_s}{dx}$, where ψ_s is the surface potential.

Since velocity saturation is relevant only in strong inversion, where the drift term dominates, we can write, in the non-saturated portion of the channel:

$$I_{ds} = Wqn_c \frac{\mu_n d\psi_s / dx}{1 + \dfrac{\mu_n d\psi_s / dx}{2v_{sat}}} \frac{dV_{CS}}{dx} \qquad (7)$$

(It is also possible to incorporate the mobility dependence on the electron density in the channel (or on the normal component of the electric field, see [14], Section 6.8.2 and expressions given below.)The channel current is obtained by integration using UCCM. In order to obtain an analytical solution, we consider an effective mobility, μ_{eff}, independent of x.

The channel current is finally written in terms of the channel charge densities at the source and drain ends:

$$I_{ds} = \frac{W}{\alpha L_{eff}} \frac{\mu_{eff} q}{1 + \delta_0 \dfrac{\mu_{eff} (n_s - n_d)}{\alpha L_{eff} v_{sat}}} \left[\eta v_T (n_s - n_d) - a \frac{n_s^2 - n_d^2}{2} \right] \qquad (8)$$

where L_{eff} is the effective channel length (including its reduction by channel length modulation) . δ_0 is a factor introduced in order to assure continuity of the derivatives at $V_{DS} = 0$.

The channel charge density at the source is obtained from UCCM using $V_{CS} = 0$. In order to calculate the inversion charge density at the drain, we cannot use the long-channel UCCM equation (1) in the saturation regime, where GCA cannot be applied in the saturated portion of the channel (near the drain). However, UCCM can be extended using the saturation voltage ($V_{CS} = V_{dsat}$) instead of $V_{CS} = V_{DS}$, which depends on the relationship used between velocity and lateral field. In order to make the model continuous, a suitable smoothing expression of the effective drain-source voltage, V_{dseff}, is needed, which tends to V_{DS} in the triode regime and to V_{dsat} in the saturation regime.

$$a(n_d - n_0) + \eta V_{th} \ln\left(\frac{n_d}{n_0}\right) = V_{GS} - V_T - \alpha V_{dseff} \qquad (9)$$

The accuracy of the high-order derivatives is critically dependent on the choice of this interpolation function. Some of the expressions of V_{dseff} proposed in the literature are:

$$V_{dseff} = V_{dsat} - V_{dsat} \frac{\log[1 + \exp A_{TS} (1 - V_{ds} / V_{dsat})]}{\log[1 + \exp(A_{TS})]} \qquad (10)$$

(see [18,19])

$$V_{dseff} = \frac{V_{ds}}{\left[1 + (V_{ds} / V_{dsat})^m\right]^{1/m}} \qquad (11)$$

(see [15])

$$V_{dseff} = V_{dsat} - \frac{1}{2}\left[V_{dsat} - V_{ds} - \delta + \sqrt{(V_{dsat} - V_{ds} - \delta)^2 + 4\delta V_{dsat}} \right] \qquad (12)$$

where A_{TS}, m and δ are fitting parameters (see [20])

The expression for the saturation voltage consistent with the Sodini velocity-field relationship is [13,14]:

$$V_{dsat} = \frac{2an_s V_L}{an_s + 2V_L} \qquad (13)$$

where $V_L = \frac{\mu_{eff}}{v_{sat}} L \qquad (14)$

This expression, (13), tends to the saturation voltage in strong inversion, but not in weak inversion, where the saturation voltage (caused by diffusion) is approximately $2V_{th}$. In order to calculate the channel charge density at the drain using the UCCM equation (1), we can use an interpolation function which tends to $2V_{th}$ in weak inversion, and to V_{dsat} in strong inversion [21] However, this interpolation function may introduce artificial peaks in the high order derivatives.

We found that the following expression for the channel charge density at the drain [16], which depends on the one calculated at the source and the expression of V_{dsat} given by (13), is very adequate for high order derivatives:

$$n_d = n_s - \alpha a V_{dseff} \left(1 + 2 \frac{\exp(-V_{ds} / V_{th})}{1 + \exp\left(a \frac{n_s}{V_{th}}\right)} \right) \qquad (18)$$

The accuracy of the higher order derivatives is critically dependent on the effective mobility model. The mobility decreases with increasing normal electric field due to the increase of phonon and surface roughness scattering. Some of the proposed expressions of the effective mobility, in terms of the effective normal field are:

$$\mu_{eff} = \frac{\mu_0}{1 + \theta E_n} \qquad (19)$$

(see, for example [6])

$$\mu_{eff} = \mu_0 (1 - \theta_\mu E_n) \qquad (20)$$

(see [14,16,17]). Here μ_0, θ and θ_μ are fitting parameters.

The normal field can be written in terms of the inversion and depletion charge densities as [13,14]:

$$E_n = \frac{qn_c/2 - q_b}{\varepsilon_{si}} \qquad (21)$$

where q_b is the depletion charge density (per unit area), which is calculated as $q_b = \gamma C_{ox} \cdot \sqrt{\phi_B + V_{CB}}$, where γ accounts for the body effect, V_{CB} is the channel voltage referred to the bulk, and ϕ_B is the semiconductor bulk potential.

A more accurate expression, which accounts separately for phonon and surface roughness scattering is [17]:

$$\mu_{eff} = \frac{\mu_0}{1 + \theta_{ph}E_n^{1/3} + \theta_{sr}E_n^2} \qquad (22)$$

In many models, the normal field used in the effective mobility expression, is calculated at the source end. However, this may be not accurate enough to model the higher order derivatives at high V_{DS}. We will use an average normal field in the effective channel, defined as:

$$E_n = \frac{q(n_s + n_d)/2 - (q_{b,s} + q_{b,d})}{2\varepsilon_{si}} \qquad (23)$$

The series resistance can be included in the expression of the effective mobility up to first order as [16,19]:

$$\mu_{effR} = \frac{\mu_{eff}}{1 + a_R} \qquad (24)$$

where μ_{eff} is the expression of the effective mobility without the series resistance and

$$a_R = \mu_{eff}C_{ox}R_T \frac{W}{L}\left(an_d + \alpha V_{dseff}/2\right) , \quad R_T \text{ being the}$$

total series resistance.

This expression of the effective mobility is used in the equation for the saturation voltage, with $V_{dseff} = V_{dsat}$, and n_d calculated at this voltage. There is no explicit solution for the saturation voltage. However, a first-order estimation, such as the long channel saturation voltage $V_{dsat} = (V_{gs} - V_T)/\alpha$, can be used in the expression of the effective mobility.

The reduction of effective channel length due to channel length modulation is obtained from a quasi-two dimensional analysis as [16]:

$$L_{sat} = l_a \log\left(\frac{C_a + \sqrt{C_a^2 + K_a^2}}{K_a}\right) \qquad (25)$$

where $C_a = V_{ds} - V_{dseff}$ and $K_a = 2l_a v_{sat}/\mu_{eff}$, l_a being the characteristic length.

The threshold voltage expression includes the DIBL effect [6]:

$$V_T = V_{T0} - \sigma V_{ds} \qquad (26)$$

where V_{T0} is the drain-bias independent threshold voltage and σ is the DIBL parameter (increasing with decreasing channel length).

The source-drain symmetry, with the resulting continuity at $V_{DS}=0$, is guaranteed by using an appropriate expression for δ_0 ($\delta_0 = \delta_L V_{dseff}/V_{dsat}$) [17](δ_L being a constant) , and an equation of the threshold voltage resulting from the linearization of the inversion charge density at the substrate; in this case, the bulk bias parameter, α, does not depend on the source-bulk voltage.

III. RESULTS

We have compared our modeling with measurements obtained from a 0.18 μm KAIST process. Most of the parameters were extracted using direct techniques, in the regimes where they are relevant. This is mainly possible because our modeling is based on charge linearization. The threshold voltage was extracted as the gate voltage, which maximizes d^2I_d/V_{GS}^2, that is, the voltage that makes $d^3I_d/V_{GS}^3=0$. The direct techniques used to extract most of the parameters are explained in [13,14].

In order to clearly identify the different mechanisms affecting the 3rd derivative, we first study the 3rd derivative of a long-channel device (Fig. 1-3). It is equivalent to study the nonlinearities of the device. Series resistance effect, velocity saturation and channel length modulation are negligible for these long-channel devices. According to the long-channel theory, $d^3I_d/V_{GS}^3=0$ in both the linear and saturation regimes. We observe in the figures that the magnitude of the 3rd derivative has a value close to zero, except in subthreshold, at the transition from below to above threshold, and at the transition from saturation to the linear regime. There is a peak value when the source end goes from weak to strong inversion and a second peak when, in long-channel devices, it is the drain end which goes from weak to strong inversion (Fig. 2). At $V_{GS}=V_T$, $d^3I_d/V_{GS}^3=0$, what means that this corresponds, in dB, to the

dip between the two peaks at low V_{DS} (Fig. 1 and 3).

We proved that some models cannot reproduce the peak found between the saturation and the linear regimes at moderate and high drain voltages. This is critically dependent on the expression of V_{dseff}. The expression (11) does not get that peak when normal values of m are used. Only using abnormally high values of m it is possible to observe the peak; however these high values of m originate artificial peaks or dips for the 3rd derivative (Fig. 1) at low V_{DS}. The expression (10) reproduces quite accurately the peak at the transition between saturation and linear regime for high V_{DS}; however, it also produce artificial peaks or dips for the 3rd derivative (Fig. 1) at low V_{DS}.

We demonstrate in Fig. 1-3 that using the third expression of V_{dseff}, we accurately reproduce all peaks for the 3rd derivative, for high and low V_{DS}, without any artificial peaks, dips nor glitches.
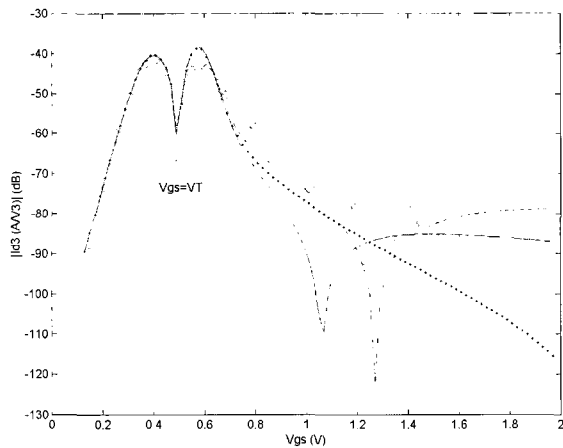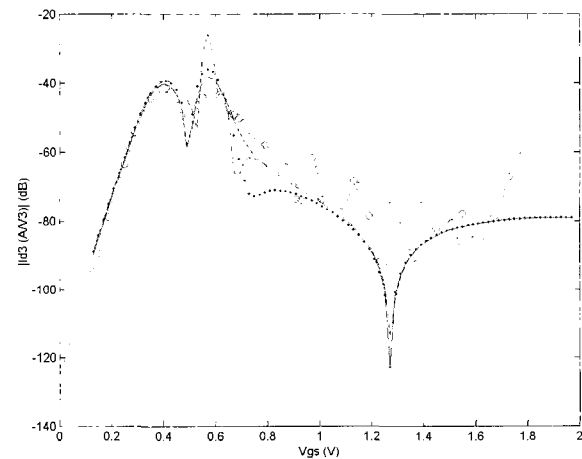

Fig. 1. Measured (symbols) and modeled d^3I_d/V_{GS}^3 (in dB) characteristics at V_{DS} =0.1 V for a transistor with L=5 μm. Model with mobility given by (19) (solid line), (20) (dotted line) and (22) (dashed line). V_{dseff} calculated according to (12)

We have also compared the effect of the different mobility models in Fig. 3. The mobility model affects the width of the peaks. The most conventional mobility model (19) is not accurate enough for the 3rd derivative. The model of Eq (20) [11] works well for the 3rd derivative at high V_{DS} (especially at moderate V_{GS}), but is far less accurate at low V_{DS} and higher V_{GS} (the values of zero-3rd derivative are significantly lower than those observed experimentally). The more complete mobility model of Eq (22) produces much better results. We note that in order to fit the width of the 1st peak at high V_{DS}

(Fig. 2) it is necessary to take into account the effect of the drain voltage on the effective normal field used in the effective mobility expression (23). Many models just use, in the effective mobility expression, the normal field at the source end, therefore ignoring the drain voltage dependence; as a result, the resulting accuracy of the 3rd derivative at high V_{ds} is lower.
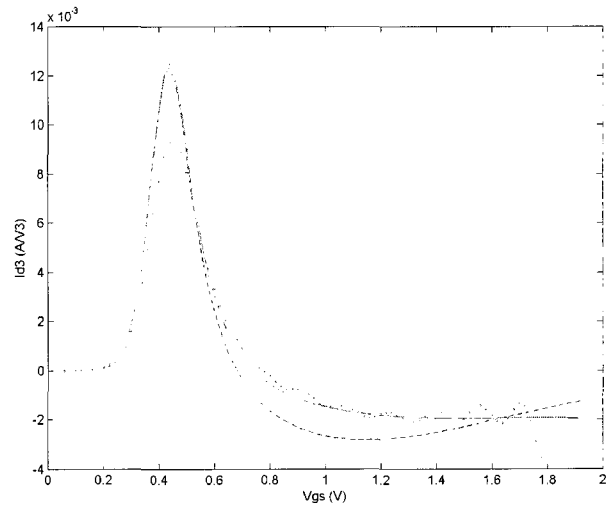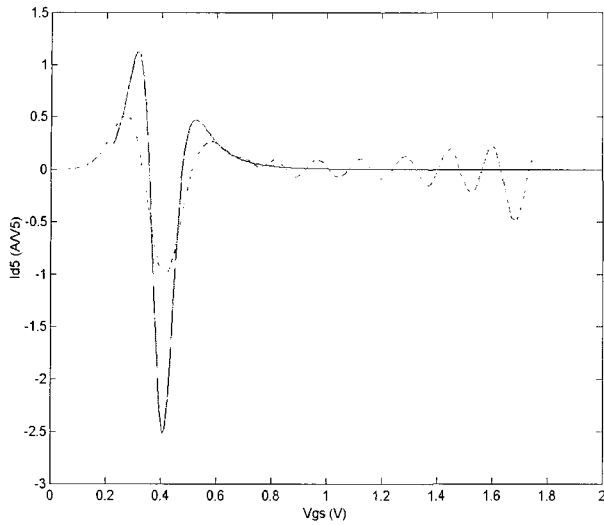

Fig. 2. Measured (dotted line) and modeled (lines) d^3I_d/V_{GS}^3 characteristics at V_{DS} =1.8 V for a transistor with L=5 μm. We have used (12) and (22). E_n calculated at the source end (dashed line) or as an average value using (23) (solid line).
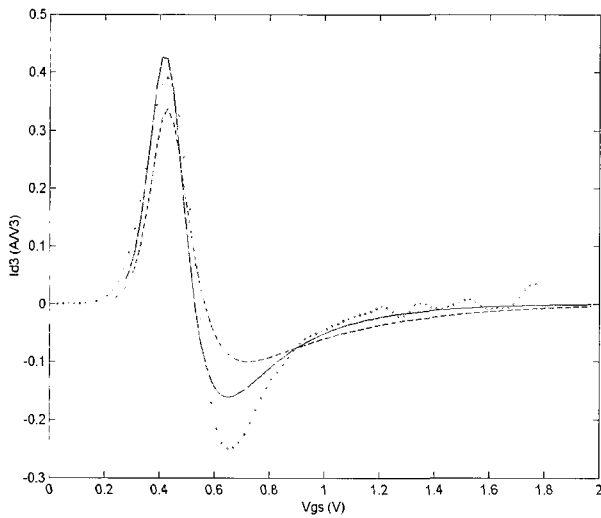

Fig. 3. Measured (symbols) and modeled d^3I_d/V_{GS}^3 characteristics (in dB) at V_{DS} =0.1 V for a transistor with L=5 μm. Mobility given by (22). V_{dseff} calculated according to (10) with A_{TS}=12 (dotted line), (11) with m=4.5 (dashed line) and (12) with δ=0.01 (solid line).

On the other hand, the fitting with the experimental 5th derivative, using the mobility model of (21) and the expression of V_{dseff} of (12), is quite acceptable (Fig. 4),

since the position of peaks are reasonably well predicted.

Fig. 4. Measured (dashed line) and modeled (solid line) d^5I_d/V_{GS}^5 characteristics at V_{DS}=1.8 V for a transistor with L=5 µm. We have used (12) and (22).

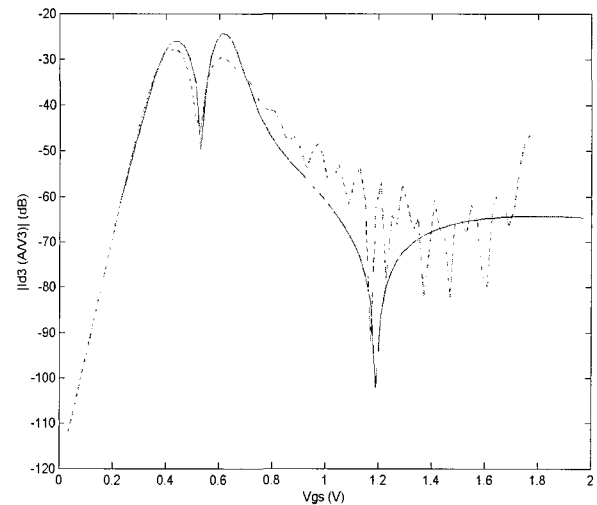**Fig. 5.** Measured (dotted line) and modeled d^3I_d/V_{GS}^3 characteristics at V_{DS} =1.8 V for a transistor with L=0.18 µm. Solid line: complete model. Dashed line: model without series resistance and channel length modulation.

The shape of the 3rd derivative is quite different for submicron and deep-submicron devices, as we note in Fig. 5-10, especially at high V_{DS}. This has to be due to short-channel effects. We did not observe anymore the negative peak at the transition between the saturation and the linear regimes; we found that it is masked by the velocity saturation effect. But we observed a new negative peak (in linear scale) in the moderate inversion

region, near threshold (Fig. 5). We demonstrated that this peak is caused by channel length modulation and the series resistance effect. The DIBL effect was also found to be significant and has an influence on the 3rd derivative in subthreshold and near threshold. Our complete model, using the suitable mobility and V_{dseff} models, and taking into account short-channel effects, fits reasonably well the experimental values of the 3rd derivative at low and high V_{DS}. The fitting of the 3rd derivative of the output characteristics (with respect to V_{DS}) is also acceptable (Fig. 8-9). Besides, we obtained a reasonable description of the 5th derivative (Fig 10).
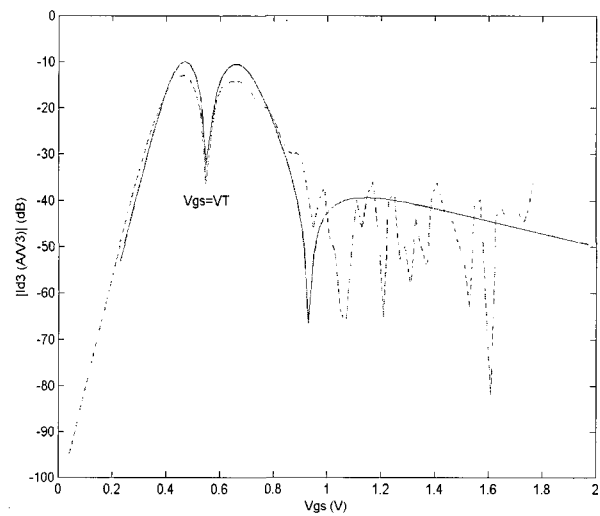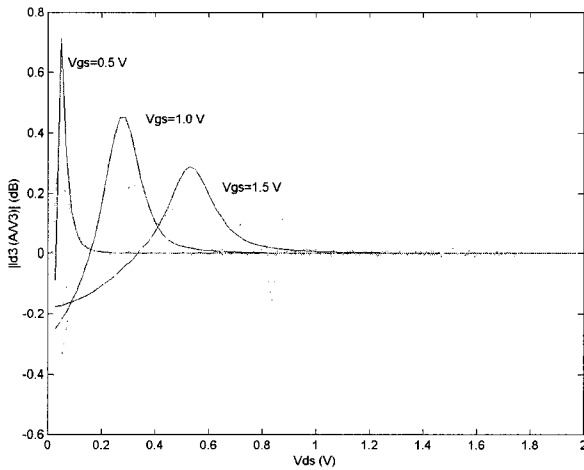

Fig. 6. Measured (dashed line) and modeled (solid line) d^3I_d/V_{GS}^3 (in dB) characteristics at V_{DS}=0.1 V for a transistor with L=0.18 µm.
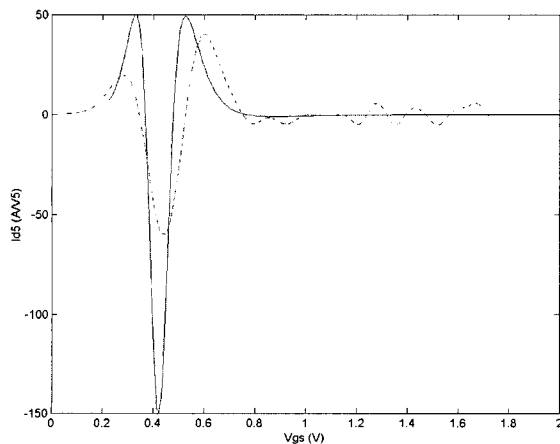

Fig. 7. Measured (dashed line) and modeled (solid line) d^3I_d/V_{GS}^3 characteristics at V_{DS}=0.1 V for a transistor with L=1.0 µm.
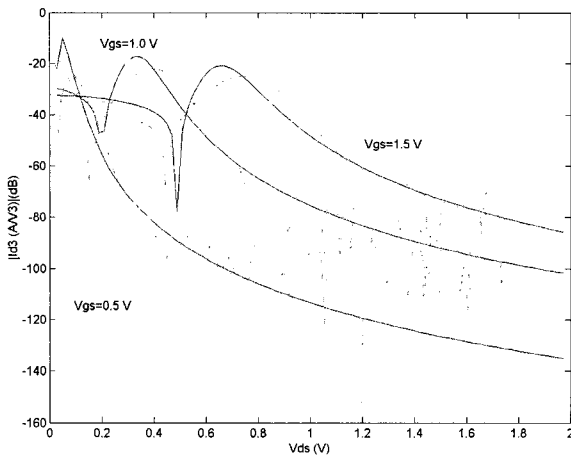
Fig. 8. Measured (dashed lines) and modeled (solid lines) d^3I_d/V_{DS}^3 (in dB) versus V_{DS} characteristics at V_{GS}=0.5, 1.0, 1.5 V for a transistor with L=1.0 μm.

Fig. 9. Measured (dashed lines) and modeled (solid lines) d^3I_d/V_{DS}^3 characteristics at V_{GS}=0.5, 1.0, 1.5 V for a transistor with L=0.35 μm.

Fig. 10. Measured (dashed line) and modeled (solid line) d^5I_d/V_{GS}^5 characteristics at V_{DS}=1.8 V for a transistor with L=0.18 μm.

IV. CONCLUSION

We have presented a compact MOSFET modeling scheme, which provides accurate descriptions of the channel current and its derivatives up to the 5th order through all operating regimes. The modeling is based on an appropriate analysis of the physical effects which determine the behaviour of the high order derivatives, and on the use of adequate smoothening functions which do not introduce any artificial peaks nor glitches in the high order derivative characteristics.

ACKNOWLEDGEMENT

REFERENCES

[1] K. Lee , "The Impact of nm CMOS Technology of Wireless Circuit and System," *Proc of the 2003 Asia-pacific Workshop on Fundamentals and Applications of Advanced Semiconductor Devices*

[2] Shin, Hyungcheol ; Minkyu Je ; Jeonghu Han ; Kwyro Lee, *Microelectronics Reliability*, vol. 43 no. pp.601-609, Apr. 2003

[3] R. Van Langevelde and F. M. Klaassen, *IEEE Trans. on Electron Devices*, vol. 44, no. 11, pp. 2044-2052, November 1997.

[4] R. van Langevelde, et al., *Electron Devices Meeting, 2000. IEDM Technical Digest. International* , Pages:807 – 810, 10-13 Dec. 2000

[5] R. van Langevelde and F. M. Klaassen, *Solid-State Electronics*, vol. 44, no., pp. 409-418, March 2000.

[6] Y. P. Tsividis, *Operation and Modeling of the MOS Transistor*, 2nd ed., New York: McGraw Hill, 1999.

[7] T. –L. Chen and G. Gildenblat, *Solid-State Electronics*, vol. 45, pp. 335-339, 2001.

[8] K. Joardar, et al., *IEEE Trans. on Electron Devices*, vol. 45, pp. 134-148, January 1998.

[9] J. –M. Sallese, et al., *Solid-State Electronics*, vol. 47,

pp. 677-683, 2003.

[10] A.I.A.Cunha, M.C.Schneider, C.Galup-Montoro, "An MOS Transistor Model for Analog Circuit Design", *IEEE Journ. Solid-State Circuits*,Vol. 33, N° 10, pp.1510-1519, October 1998.

[11] C. -K. Park, et al., "A unified current-voltage model for long-channel nMOSFETs," *IEEE Trans. on Electron Devices*, vol. 38, pp. 399-406, February 1991.

[12] M. S. Shur, T. A. Fjeldly, T. Ytterdal and K. Lee, "Unified MOSFET model, *"Solid-State Electronics*, vol. 35, no. 12, pp. 1795-1802, December 1992.

[13] K. Lee, M. Shur, T. A. Fjeldly and T. Ytterdal, *Semiconductor Device Modeling for VLSI*, Prentice-Hall, 1993.

[14] T. A. Fjeldly, T. Ytterdal and M. Shur, *Introduction to Device Modeling and Circuit Simulation*, New York, John Wiley & Sons, 1998.

[15] B. Iñíguez and E. García-Moreno, *IEEE Transactions on Computer-Aided Design of Integrated Circuits and Systems*, vol. 14, no. 2, pp. 163-166, February 1995 .

[16] B. Iñíguez and E. García-Moreno , *Analog Integrated Circuits and Signal Processing* (Kluwer), vol. 13, no. 3, pp. 241-259, July 1997.

[17] S. B. Chiah, et al., *IEEE Electron Device Letters*, vol. 25, no. 5, May 2004

[18] C. C. McAndrew, B. K. Bhattacharyya and O. Wing, *IEEE Electron Device Letters*, vol. 12, pp. 565-567, October 1991.

[19] N. D. Arora, et al., *IEEE Trans. on Electron Devices*, vol. 41, pp. 988-997, June 1994.

[20] Y. Cheng, et al., *IEEE Trans. on Electron Devices*, vol. 44, pp. 277-287, February 1997.

[21] J. A. Power and W. A. Lane, *IEEE Trans on Computer-Aided Design*, vol. 11, pp. 1418-1425, November 1992

The authors' biography's and photo's are not available at the time of publication.